Odor maps of aldehydes and esters revealed by functional MRI in the glomerular layer of the mouse olfactory bulb

Fuqiang Xu[†‡§], Nian Liu[‡], Ikuhiro Kida[†], Douglas L. Rothman[†], Fahmeed Hyder[†], and Gordon M. Shepherd[‡]

Departments of [†]Diagnostic Radiology and [‡]Neurobiology, Magnetic Resonance Research Center, Yale University, New Haven, CT 06510

Edited by Marcus E. Raichle, Washington University School of Medicine, St. Louis, MO, and approved July 16, 2003 (received for review May 13, 2003)

Odorant identity is believed to be encoded in the olfactory bulb (OB) by glomerular activity patterns. It has not yet been possible to visualize and compare entire patterns for different odorants in the same animal because of technical limitations. For this purpose we used high-resolution functional MRI at 7 T, combined with glomerular-layer flat maps, to reveal responses to aliphatic homologues in the mouse OB. These odorants elicited reproducible patterns in the OB, with the medial and lateral regions containing the most intense signals. Unexpectedly, in view of the symmetrical projections of olfactory receptor neurons to medial and lateral glomeruli, the activity patterns in these regions were asymmetrical. The highly activated medial and lateral areas were shared by homologous members, generating a conserved ''family signature'' for a homologous series. The moderately active areas, including the dorsal region that has been extensively studied by optical imaging, were more sensitive to the length of the carbon chain, producing more subtle features of individual members and different changing trends among homologues. The global mapping with functional MRI not only extended previous studies but also revealed additional rules for representation of homologues in the OB. Insights into possible relations between the functional patterns, molecular projections, and odor perception may now be obtained based on the global from the olfactory epithelium to the OB glomerular activity patterns.

Evidence is increasing that odors elicit specific spatial activity patterns in the glomerular layer of the olfactory bulb (OB) that encodes information of olfactory stimuli (1–15). A given odor can activate many glomeruli, and a glomerulus can be activated by many odorants, in agreement with molecular, cellular, and physiological studies on the responses of olfactory receptor neurons (16–20). Highly activated glomeruli frequently cluster together, forming module, or focus, domains (10, 12, 21, 22). Mapping with 2-deoxyglucose (2DG) shows that the domains tend to be paired in medial and lateral OB regions (8), similar to the pairing of receptor projections to the glomeruli (23–25).

The hypothesis that the patterns are involved in odor coding (26) is supported by numerous studies showing that activated glomeruli or glomerular regions shift with differences in chemical structure (7, 8, 11, 12, 14, 15, 27). However, further analysis is limited by the methods currently available. Global methods (such as 2DG, which reveals patterns throughout the entire glomerular layer) test single odors in terminal experiments, preventing comparison of responses to different odors in the same animal. Optical methods, involving recording individual glomerular responses to different odors in the same animal, are limited to observations on the accessible dorsal surface, a fraction of the entire OB.

To overcome these limitations, we have developed functional MRI (fMRI) with high spatial resolution, together with a method for making flat maps of the glomerular layer. We focus here on how molecules of different carbon chain lengths belonging to the same homologous series are encoded by using aldehydes and esters as model odorants. The results extend previous studies on aliphatic odorants by showing that the major activity is in medial and lateral regions and that the patterns shift with carbon chain length. Asymmetrical medial and lateral activity contrasts with the symmetrical projection of olfactory receptor neurons to the OB, indicating functional differences in the two projection pathways. The results give insights into possible relations between the functional patterns, molecular projections to the OB, and odor perception.

Materials and Methods

Animal Preparation. Male CD-1 mice (30–40 g) were anesthetized with 1–2% halothane, and the skin overlying the OB was removed to expose the skull. Before the mouse was placed in the magnet the anesthesia was switched to urethane (i.p. 1.0 $mg \cdot g^{-1}$ initial; 0.1 $mg \cdot g^{-1} \cdot h^{-1}$ supplemental). The surgical procedure was approved by the Yale Animal Care and Use Committee (YACUC no. 10004).

Odor Delivery. The odor-delivery system was made of Teflon and glass with a dead volume of 5 ml. Mineral oil was used as the solvent to prepare the odor solution. The flow rate of the extra-pure air passing over the odorant solution was kept at 3 liters/min, generating odorized airflow at selected odor concentrations. The gas-phase concentrations were calculated from the mass decrease of odorant over a period of 10 min under the same conditions. The concentrations of the solutions were adjusted so that the vapor concentrations of different odorants were approximately the same. All chemicals were from Sigma.

Anatomical MRI and fMRI. Experiments were performed on a horizontal-bore 7-T Bruker spectrometer (Bruker, Billerica, MA). All image orientations were coronal, and contiguous slices were obtained to cover the entire OB. The magnetic field homogeneity was optimized by manual shimming. T_1-weighted fast low-angle single-shot (FLASH) anatomical images were obtained (image dimension = 128 × 128 pixels; in-plane resolution = 100 × 100 μm; slice thickness = 200 μm; repetition delay = 5.0 s; echo time = 16 ms; flip angle = 90°) with variable inversion recovery weighting per slice. Each multislice fMRI experiment consisted of a series of 128 $T_{\frac{1}{2}}$-weighted FLASH images (image dimension = 64 × 64 pixels; in-plane resolution = 200 × 200 μm; slice thickness = 200 μm; repetition delay = 400 ms for 16 slices; echo time = 16 ms; flip angle = 5–15°). In each experiment, 16 dummy scans per slice were carried out before data acquisition. The animals were rested at least 20 min between successive experiments to avoid adaptation.

This paper was submitted directly (Track II) to the PNAS office.

Abbreviations: 2DG, 2-deoxyglucose; fMRI, functional MRI; OB, olfactory bulb; SCC, spatial correlation coefficient.

Data deposition: The fMRI data have been deposited in the fMRI Data Center, www.fmridc.org (accession no. 2-2003-11499).

[§]To whom correspondence should be addressed at: N136 TAC (MRRC), 1 Gilbert Street, New Haven, CT 06510. E-mail: fuqiang.xu@yale.edu.

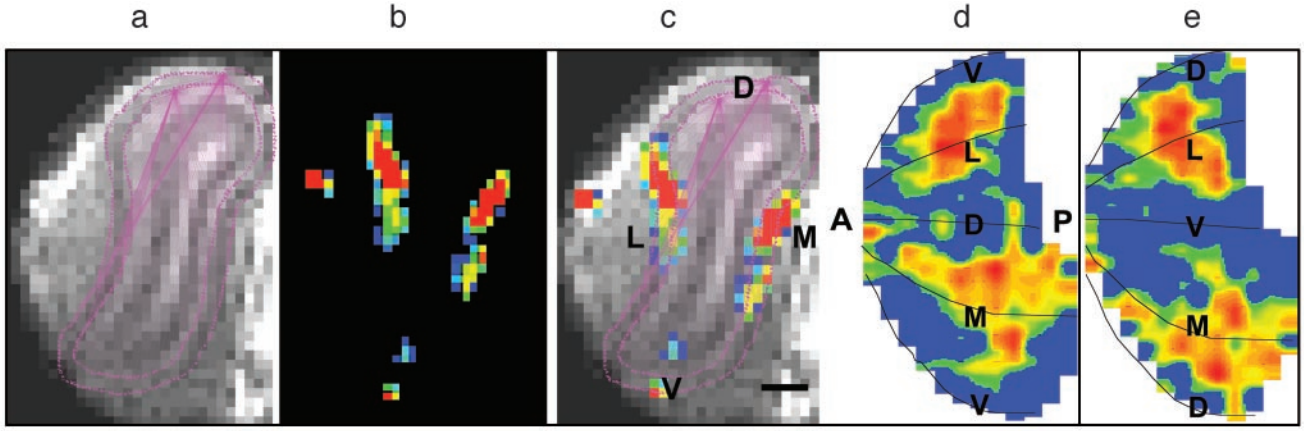

Fig. 1. Illustration of method for constructing flat maps of fMRI signal in the glomerular layer by using the software program ODORMAPBUILDER. (*a*) Glomerular layer outlined on the anatomical MRI image of the OB. (*b*) fMRI signal from a typical trial of odor stimulation (heptanal). (*c*) Superposition of *b* over *a*. (Scale bar = 500 μm.) (*d*) Dorsal-centered map. (*e*) Ventral-centered map. A, anterior; P, posterior; D, dorsal; M, medial; V, ventral; L, lateral.

Data Processing. Details of data processing have been described (6). For each experiment, the mean image of the prestimulation "baseline" images was subtracted from the "stimulation" images on a pixel-by-pixel basis to produce $\Delta S/S$ (fractional change in fMRI signal) and student t maps. Usually, two to four frames in the stimulation period were averaged to give a single functional map. Each linearly interpolated $\Delta S/S$ map was overlaid onto the corresponding anatomical image to reveal the location of activity in the OB layers. Flat maps of the activity throughout the glomerular layer were constructed similar to those used in 2DG and c-fos studies (8, 13, 26). A software program called ODORMAPBUILDER was specially designed for adapting this approach to the anatomical MRI and fMRI data, as shown in Fig. 1. In brief, for each slice, the fMRI signal was overlaid on the anatomical MRI image, and the signals in the glomerular layer were extracted and flattened. Every flattened glomerular layer was then consecutively placed and linearly interpolated to create the glomerular sheet. Detailed description of the method has been presented elsewhere (28). With the spatial resolution in this study, the major bulb layers could be readily separated. A given pixel likely contained several glomeruli, and possibly, a small amount of neighboring nonglomerular tissue. The columnar-like arrangement of a glomerular unit across the OB layers, and the tendency of neighboring glomeruli to receive input from similar receptor neurons (29), make the activity in neighboring pixels highly correlated (21). The fMRI patterns in this report should therefore closely reflect the activity pattern in the glomerular layer. More detailed correlations of the blood oxygenation level-dependent signal with individual glomeruli remain to be analyzed.

To determine the similarity between odor maps, a previously described spatial correlation analysis was used (30). The method takes all pixels within the OB into consideration, because even the pixels not significantly activated affect the spatial feature of a pattern. A pixel in an odor map has a value of either 1 (above threshold) or 0 (below threshold). When two odor maps, A and B, are compared (expressed as A∩B), a given pixel must belong to one of the four different categories, [1, 1], [1, 0], [0, 1], and [0, 0], where the values in each square bracket represent intensities of that pixel in odor maps A and B, respectively. $N_{[1,1]}$, $N_{[1,0]}$, $N_{[0,1]}$, and $N_{[0,0]}$ are the total counts of the pixels in the corresponding categories. The spatial correlation coefficient (SCC) is defined by either

$$\mathrm{SCC} = \frac{N_{[1,1]}N_{[0,0]} - N_{[1,0]}N_{[0,1]}}{(N_{[1,0]} + N_{[1,1]})(N_{[1,0]} + N_{[0,0]})}$$

when $N_{[1,1]}N_{[0,0]} > N_{[1,0]}N_{[0,1]}$, or

$$\mathrm{SCC} = \frac{N_{[1,1]}N_{[0,0]} - N_{[1,0]}N_{[0,1]}}{(N_{[1,0]} + N_{[1,1]})(N_{[0,1]} + N_{[1,1]})}$$

when $N_{[1,1]}N_{[0,0]} < N_{[1,0]}N_{[0,1]}$ and $N_{[1,1]} < N_{[0,0]}$. If $0.2 < \mathrm{SCC} < 1.0$, a significant degree of domain overlap occurs ($P < 0.01$). If $-0.2 > \mathrm{SCC} > -1.0$, a significant degree of domain segregation or avoidance from each other occurs ($P < 0.01$). If $0.2 > \mathrm{SCC} > -0.2$, no significant correlation occurs, indicating a near random relation. It has been shown that thresholding usually does not significantly affect the SCC values (31). In most cases, odor maps A and B were obtained with different odorants. However, for tests of reproducibility, maps A and B were obtained with the same odorant in different exposures.

Results

Construction of Odor Maps. The fMRI signal changes were correlated with the specific layers of the OB by superimposing them over the anatomical MRI image (Fig. 1 *a–c*). We focused on activity in the glomerular layer (between the two dotted lines in Fig. 1 *a* and *c*). The signals in the glomerular layer of each slice were extracted, unfolded, and reconstructed from contiguous coronal sections into a two-dimensional odor map of the glomerular sheet (Fig. 1 *d* and *e*). The odor map could be viewed from different perspectives; for example, dorsal centered (Fig. 1*d*) or ventral centered (Fig. 1*e*). Dorsal-centered maps were used in this report to facilitate comparisons with optical imaging data in the dorsal OB.

Global Patterns of Aldehyde Homologues. ***General features.*** Aliphatic homologues are compounds with the same functional groups but different carbon chains. To reveal how they are represented in the OB, the patterns elicited by aldehydes with a straight chain of 4–8 carbon atoms (C4–C8) in the same mouse were mapped with fMRI. Aldehydes are of particular interest because of recent molecular and cellular imaging studies in the epithelium and OB (9, 11, 14, 18, 19, 32–35) and the limited information about their global patterns (8).

Comparisons of the activity maps in Fig. 2*a* demonstrate several basic characteristics. All aldehydes activated significant portions of the glomerular layer. The topography of the maps evolved regularly with the carbon-chain length. The signal increased both in area and in intensity with carbon number, peaking at C7 (Fig. 2*b*). A striking feature was that the main activity occurred in broad regions of the medial and lateral

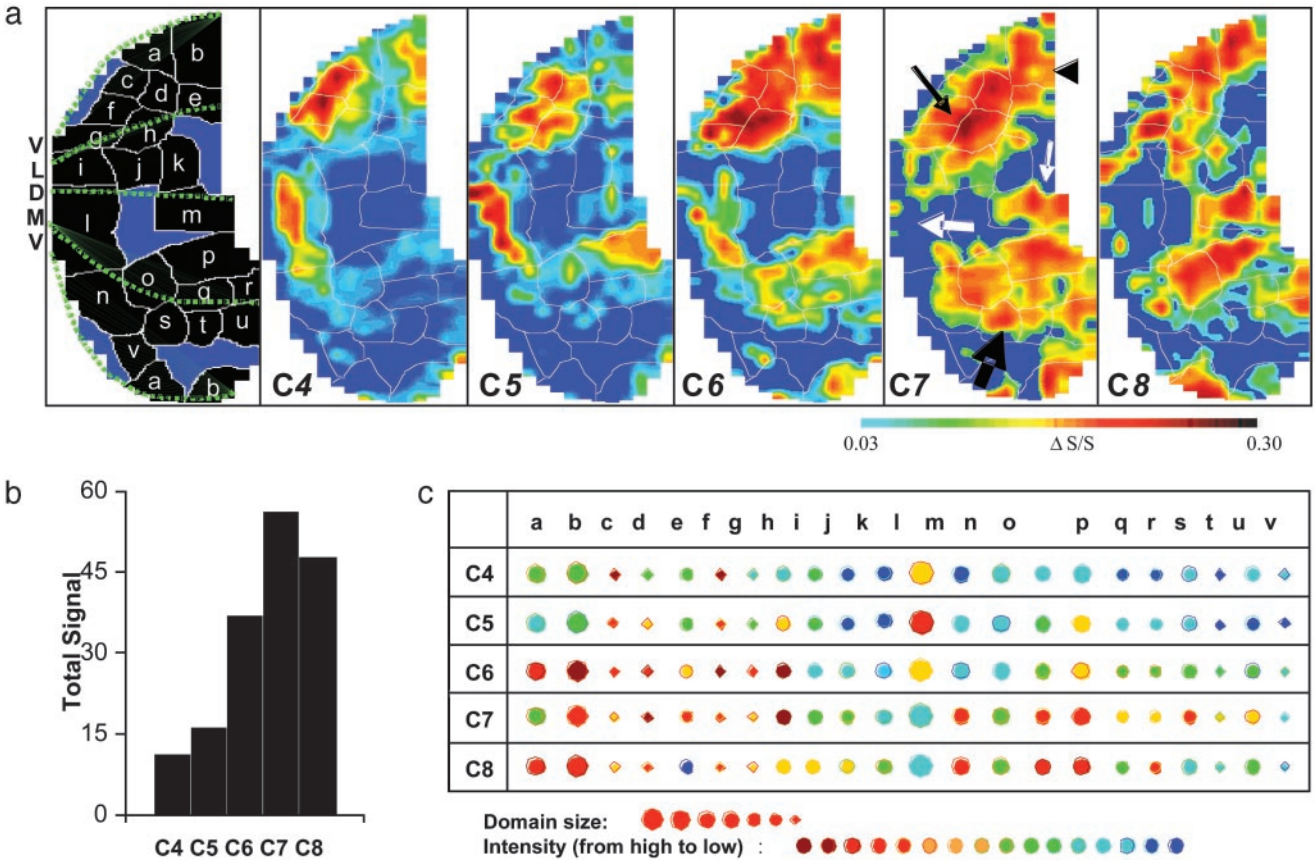

Fig. 2. Global activity patterns in the glomerular layer for aliphatic aldehydes in the same mouse. (*a*) Odor maps of aldehydes: C4 (butanal), C5 (pentanal), C6 (hexanal), C7 (heptanal), and C8 (octanal). Modules are identified (*Left*) and overlaid on the odor maps (as thin white lines). (*b*) Effects of carbon number on total signal. (*c*) Modular comparison of odor maps. Exposure duration, 2 min; interexposure, ≈20 min.

regions. The anterior lateral surface (fine black arrow in Fig. 2*a*) was highly activated by all tested aldehydes, whereas the intensities in the medial and posterior lateral surface (thick black arrow and arrowhead, respectively, in Fig. 2*a*) increased most notably with carbon number. The difference in lateral and medial responses was observed in all animals (data not shown). In the dorsal region, shorter-chain aldehydes activated the anterior part, whereas longer carbon chains activated the posterior part (thick and fine white arrows, respectively, in Fig. 2*a*). In all maps, the activity in the medial side was located at more posterior regions than that in the lateral side.

Modular comparison. To compare the maps more closely, a modular analysis was carried out, which was similar to the approach used to characterize 2DG maps (8, 27). Modules were defined as local areas activated by at least two members of the homologues, within which the intensity averaged over all pixels shifted as regularly as possible with carbon chain length. The results are outlined in Fig. 2*a Left*, and overlaid on the C4–C8 activity patterns as thin white lines. Comparisons of the intensity and size of the modules in different maps are summarized in Fig. 2*c*. For many of the modules, the relative activity elicited by the aldehydes evolved regularly with carbon chain length, whereas other modules altered their activities irregularly with carbon number. Within this framework, almost all possible activity-changing trends were observed. In agreement with these visual observations, statistical analysis (see Fig. 3) showed that maps of aldehydes with one carbon difference were highly similar and that the similarity decreased as the difference in carbon number increased.

Quantitative analysis. To supplement the modular analysis, quantitative SCC was used to assess the spatial correlations between pairs of patterns (see *Materials and Methods*). We focused more on areas with higher intensity activity, on the assumption that they reflect the activation of receptors that are more sensitive to a given odor and statistically contribute more to the pattern topography. For this purpose, the odor maps were thresholded at the 50th percentile of intensity to divide the map into two tiers, lower and higher than 50%, L_{50} and H_{50}. The H_{50} was further divided into three submaps according to intensity (Fig. 3*a*: I_1, 84–100%; I_2, 68–83%; and I_3, 51–67% of maximum intensity) and compared. An example of the method for analyzing the degree of spatial correlation between two maps is shown in Fig. 3*b*. Map A is the I_1 submap for C4 (butanal) and map B is the I_1 submap for C5 (pentanal). The total numbers of the four different categories of pixels, $N_{[1,1]}$, $N_{[1,0]}$, $N_{[0,1]}$, and $N_{[0,0]}$, represented by red, black, green, and blue, respectively, in A∩B of Fig. 3*b*, were used to calculate the corresponding SCC.

Detailed analysis using SCC is presented in Fig. 3*c* for the typical set of data shown in Fig. 2*a*. Six types of comparison between submaps were carried out: I_1 submap of one odorant with the I_1 ($I_1 \cap I_1$, black bars), I_2 ($I_1 \cap I_2$, red bars), I_3 ($I_1 \cap I_3$, green bars), and L_{50} submap of another odorant ($I_1 \cap L_{50}$, blue bars); I_2 submap of one odorant with the I_2 submap of another odorant ($I_2 \cap I_2$, orange bars); and I_3 submap of one odorant with the I_3 submap of another odorant ($I_3 \cap I_3$, indigo bars). To examine the maps of aldehydes with the smallest difference, C4 and C5 were taken as an example. The areas with the highest signal intensity were highly conserved between the two maps (black bar in C4/C5). In agreement with this result, these areas

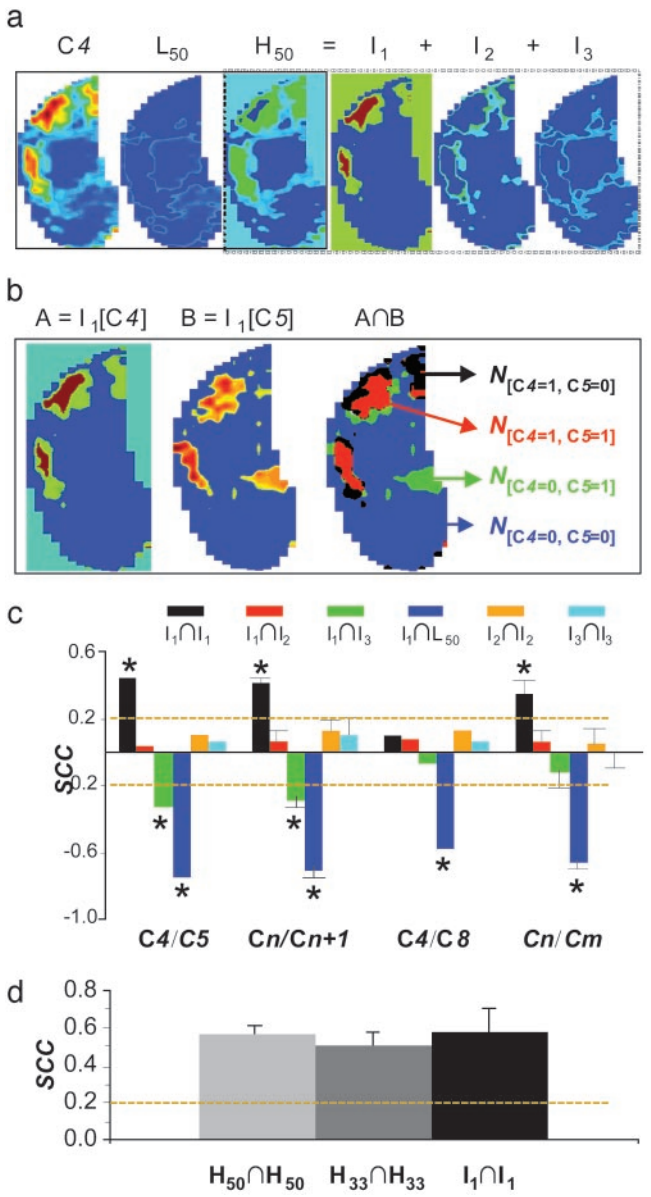

Fig. 3. Comparison of odor submaps defined by different activation levels. (*a*) The butanal odor map (C4) was divided into lower (L_{50}) and upper (H_{50}) halves by thresholding at the 50th intensity percentile. The H_{50} was then divided into three levels: I_1, 84–100% (highest intensity); I_2, 67–83% (medial intensity); and I_3, 50–66% (low intensity). (*b*) Example to demonstrate the analysis of spatial correlation (SCC; see *Materials and Methods*) between submaps for different odors: A is the I_1 submap for C4 and B is the I_1 submap for C5. The SCC value is calculated from the total counts of the four different pixel categories, $N_{[1,1]}$, $N_{[1,0]}$, $N_{[0,1]}$, and $N_{[0,0]}$, represented by red, black, green, and blue, respectively. (*c*) A detailed analysis using SCC with data in Fig. 2*a*. C4/C5, the comparison between more similar butanal and pentanal maps; C*n*+*1*, averaged values for all comparisons between the maps of aldehydes with one carbon difference ($n = 4$, 5, 6, and 7); C4/C8, the comparison between less similar butanal and octanal maps; C*n*/C*m*, averaged values for all possible comparisons between the maps of aldehydes shown in Fig. 2*a* (m, $n = 4$, 5, 6, 7, and 8; $m \neq n$). $I_1 \cap I_1$ (black bars), $I_1 \cap I_2$ (red bars), $I_1 \cap I_3$ (green bars), and $I_1 \cap L_{50}$ (blue bars) are for comparisons of I_1 submap of one odorant with the I_1, I_2, I_3, and L_{50} submap of another odor map, respectively; $I_2 \cap I_2$ (orange bars), the comparisons between the I_2 submaps of different odor maps; and $I_3 \cap I_3$ (indigo bars), the comparisons between the I_3 submaps of different odor maps. The dotted yellow lines around SCC values of ±0.2 depict the significant correlation at $P = 0.01$. (*d*) Tests of reproducibility of activity patterns for aldehydes using the SCC calculation. Reproducibility was assessed from SCC values at three different thresholding levels: top 50% ($H_{50} \cap H_{50}$), top 33% ($H_{33} \cap H_{33}$), and top 16.7% ($I_1 \cap I_1$). The plotted values represent the averaged SCC from pentanal to octanal.

were significantly segregated from the areas with low signal intensities (I_3 and L_{50}, green and blue bars in C4/C5). All of the other correlations involving submaps with moderate intensity (I_2 and I_3) were not significant, suggesting these areas are sensitive to carbon chain length. The averaged values of all comparisons for the maps with one carbon difference demonstrated identical results (see C*n*+*1*). On the other hand, C4 and C8 had the largest carbon difference for the tested aldehydes. Accordingly, their maps were less correlated (see C4/C8). The only statistical significant conclusion was that the areas with the highest intensity (I_1) were segregated from the L_{50} of the other map, indicating a degree of similarity between the C4 and C8 maps.

Finally, the analysis of these aldehydes as a family was performed by averaging the SCC of all 10 possible pairwise comparisons for each of the six types (C*m*/C*n* in Fig. 3*c*). The areas with the highest intensity (I_1) were significantly correlated with each other, i.e., conserved among the homologous members. The spatial correlation and conservation of the areas with high intensity appear to underlie the patterns with family features among homologous maps. The moderately activated areas, on the other hand, have a near random correlation, indicating that these areas are more affected by the length of carbon chain and thus produce more subtle and specific characteristics of each individual member in addition to the shared family features.

Pattern reproducibility. fMRI mapping permitted us to assess quantitatively the reproducibility of the global patterns in the entire OB from the same animal. Fig. 3*d* shows the SCC assessment of the spatial correlation at three different thresholding levels: top 50% ($H_{50} \cap H_{50}$), top 33% ($H_{33} \cap H_{33}$), and top 16.7% ($I_1 \cap I_1$). The spatial correlations between the maps of the same odorants were relatively high (SCC > 0.5), and indeed were not significantly affected by thresholding, as reported in visual cortex for activation with the same stimuli (31). Furthermore, the averaged value for the correlations between the maps of the same odorants was significantly higher than that for the most similar maps of different odorants.

Local Patterns in the Dorsal Bulbar Region. Responses in the anterior dorsal OB region have been extensively examined by optical imaging methods (7, 9, 11, 12, 14, 15, 32), which have shown differential responses of individual glomeruli to different aldehydes. As shown by Fig. 2*a* (indicated by a thick white arrow), the signal in module l was maintained from C4 to C5, and then decreased at longer chain lengths; by comparison, the signal in module i, which is located more laterally, is weakest for shorter chain lengths and highest for C7 and C8. Taking into account different experimental conditions (odor concentration, etc.) in these different studies, the fMRI patterns in the dorsal OB thus showed systematic shifts with odorant chemical structure.

Global Patterns of Ethyl Acetate and Amyl Acetate. To test whether the properties of the maps revealed above were specific to aldehydes or common to different homologous series, the global patterns for two esters with different carbon chains, ethyl acetate and amyl acetate, were obtained (Fig. 4). Similar to aldehyde homologues, the ester with the longer amyl group activated larger areas with higher intensity levels and more symmetrical signals in the medial and lateral regions (Fig. 4 *a* and *c*, with the same threshold). By thresholding the ethyl acetate (Fig. 4*b*) and amyl acetate (Fig. 4*c*) maps at the 50th percentile, significant spatial correlations and overlap were noted (SCC = 0.44 and 72% overlap) between the two patterns (Fig. 4*d*). However, the absolute size and intensity appeared to vary in the two maps (Fig. 4 *b* and *c*). It thus appeared that similar trends were found for ester patterns as for aldehydes (Fig. 2).

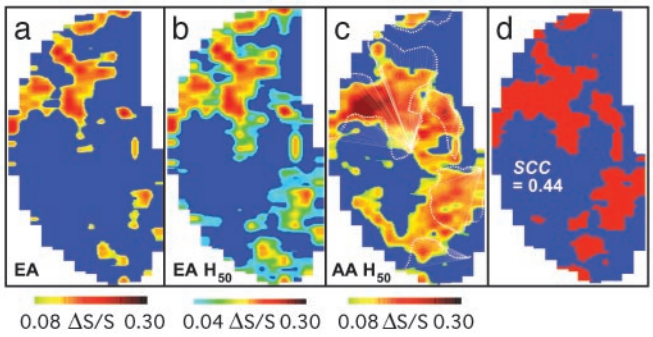

Fig. 4. Global activity patterns of esters. (*a*) Map of ethyl acetate. (*b*) Map in *a* thresholded at the 50th percentile. (*c*) Map of amyl acetate thresholded at the 50th percentile, with the major foci of ethyl acetate in white contours. (*d*) Overlapped areas between *b* and *c*. Exposure duration, 2 min; interexposure period, ≈20 min. AA, amyl acetate; EA, ethyl acetate.

Discussion

Homologues Are Represented by Pattern Similarities, and Their Carbon Numbers Are Represented by Subtle Differences. The patterns of the aliphatic aldehydes tested (Fig. 2*a*) suggest several principles involved in their representation within the entire glomerular layer. Although different molecules produced different global patterns, the patterns showed similarities when their most active regions were compared (Fig. 3*c*). This finding suggests that the most active regions together constitute a "family signature" for a given odor type. The patterns tended to differ in their moderately activated regions, suggesting that carbon number is represented by these differences (Fig. 3*c*). These considerations are consistent with the idea that the receptors with the highest affinities for aldehydes give a family signature of activated glomeruli, whereas receptors with lower affinities respond differentially to varying carbon lengths, depending on the fit with their binding pockets (19, 35). Other studies are necessary to assess the degree to which other types of homologous series produce family signatures that are distinct from these two series.

Activity Is Most Prominent in the Medial and Lateral OB Regions. The results extend 2DG studies (8, 26) in showing that the main sites of activity elicited by aliphatic homologues are distributed in the medial and lateral regions of the glomerular layer (see Fig. 2*a*). These regions are also favored by many other types of odors (8, 10). These medial and lateral areas of functional activity are believed to be related to the medial and lateral projections of olfactory receptors (but see below).

Medial-Lateral Activity Is Asymmetrical. This article has revealed a functional asymmetry between the medial and lateral activity domains in representing different homologues (see Figs. 2*a* and 4). With shorter chain lengths, anterolateral activity predominates; with longer chain lengths, medial activity emerges strongly. This observation contrasts with the evidence that receptor neurons expressing a given type of olfactory receptor project in a stereotyped manner to glomeruli on the medial and lateral sides of the OB (24, 25). Thus, the ability of fMRI to map activity across the entire OB in the same animal for structurally related odorants shows that the functional map is not stereotyped and restricted to reflecting simply the anatomical substrate of projections, but is dynamic, reflecting, in addition, the physiological properties of the responding elements.

An asymmetry has been suggested by other studies at different levels of the system (36–38). In the epithelium, receptor neurons projecting to the medial and lateral glomeruli are located in the dorsomedial and ventrolateral parts of the olfactory epithelium, respectively (39–41). The two different locations in the epithelium have different airflow and odorant absorption rates (42–45). Thus, neurons expressing the same olfactory receptor protein may sense different concentrations of the same olfactory stimulus, which is consistent with electrophysiological recordings and optical imaging of the olfactory epithelium along the rostrocaudal and dorsoventral axis (46–48). In the OB, regulation mechanisms in the medial and lateral OB may be different. Expression of tyrosine hydroxylase, the key regulator of catecholamine synthesis, is suppressed by naris-occlusion, more in the anteromedial than in the posterolateral region (49). These factors could be part of the reason for the slight variability of temporal response among glomeruli (14, 32) and the corresponding pattern shift with time (32). The time-dependent shift might be used to code temporal information of olfactory stimulus.

Significance of Dorsal Region Activity. The fMRI results extend 2DG studies showing that, compared with the medial and lateral regions of activity, much more limited activity is seen in the dorsal glomerular regions, which presumably include those observed with optical methods (7, 9, 11, 12). Those studies have documented shifts in individual activated glomeruli with different aldehydes (9, 11), which are consistent with the present fMRI results. Statistical analysis demonstrated that the areas with moderate signal in the aldehyde maps were sensitive to carbon chain length (Figs. 2*a* and 3*c*). The associated systematic shifting in the dorsal surface pattern would imply a fractal-like representation of odor identity in different areas. In other words, different areas shift similarly in relation to changes in given molecular properties, reflecting a redundancy at different levels of a global pattern. Future ultrahigh-spatial-resolution fMRI data are needed to confirm this hypothesis at the glomerular level.

Possible Correlations of Odor Maps with Behavior and Perception. The results have shown an increase in total activity pattern with increasing aldehyde chain length from C4 to C7. Evidence reveals that the behavioral and psychophysical thresholds for aldehyde detection decrease over this range (50, 51). Detailed studies with threshold stimuli will be necessary to test this correlation.

The fMRI results are relevant to the interpretation of effects of ablation studies on odor perception. The fact that large ablations of the OB have little effect on odor perception (52) may be accounted for by the widespread nature of the medial and lateral glomerular activity patterns and the redundancy built into their odor representation. A similar explanation appears to explain why ablations of the dorsal olfactory bulb have little effect on aldehyde discrimination (53). As shown in this article, the dorsal region has only weak to moderate activity, whereas the major representation is in the lateral and medial regions. Ablating the dorsal surface would not significantly affect the general representation, thus the persistent discriminability of these odors.

Advantages and Nature of fMRI Mapping. The present results illustrate the ability of fMRI to test different odorants for their odor maps in the same animal, as shown in the rat (6). They demonstrate that the method can now be applied to the mouse OB, a much smaller structure, but one nonetheless in which resolution has been achieved at the laminar level (cf. ref. 22). This finding opens the way to application of fMRI to gene-targeted animals.

Like most other activity-mapping methods, the fMRI signal does not discriminate possible cellular contributions to these patterns (54), which is unlikely to affect the conclusions from the analysis focusing on higher activity areas. The fMRI signal reflects the total energy usage, thus a pixel of high intensity

represents a large change in energy consumption (55). Although presynaptic inhibitory activities exist in the glomerular layer, they consume a small portion of total energy (56). The glomerular activity is dominated by the excitatory actions of the converging sensory axons (57). If a glomerulus is not highly activated by receptor neurons, but receives strong inhibition from nearby glomeruli, it will have a detectable, but unlikely a strong, fMRI signal.

Mapping with fMRI, as implemented by the present flat-map program, can make possible visual and quantitative comparison of global glomerular patterns elicited by different odorants or concentrations in the same animal. Because the same set of fMRI data contains the responses from the entire OB, these methods can be easily applied to obtain the patterns in the other OB layers for correlation with the glomerular patterns, although we have focused here only on the glomerular layer. The results reported here suggest that the global pattern revealed by fMRI can shed light on the possible relations between the functional patterns, molecular projections, and odor perception.

We thank the engineers of the Magnetic Resonance Research Center at Yale for technical support and Drs. C. A. Greer and R. G. Shulman for advice. This research is supported by National Institutes of Health Grants DC-00086 (to G.M.S.), NS-32126 (to D.L.R.), NS-37203 (to F.H.), DC-03710 (to F.H.), MH-67528 (to F.H.), U24 DK59635 (Yale Mouse Metabolic Phenotyping Center), National Science Foundation Grant DBI-0095173 (to F.H.), the Human Brain Project (National Institute on Deafness and Other Communication Disorders, National Institute of Mental Health, National Institute of Neurological Disorders and Stroke, and National Institute on Aging), and the Office of Naval Research (Multi-University Research Initiative).

1. Hildebrand, J. G. & Shepherd, G. M. (1997) *Annu. Rev. Neurosci.* **20,** 595–631.
2. Sharp, F. R., Kauer, J. S. & Shepherd, G. M. (1975) *Brain Res.* **98,** 596–600.
3. Kauer, J. S. (1988) *Nature* **331,** 166–168.
4. Guthrie, K. M., Anderson, A. J., Leon, M. & Gall, C. (1993) *Proc. Natl. Acad. Sci. USA* **90,** 3329–3333.
5. Joerges, B. A., Kutterner, A., Galizia, C. G. & Menzel, R. (1997) *Nature* **387,** 285–288.
6. Yang, X., Renken, R., Hyder, F., Siddeek, M., Greer, C. A., Shepherd, G. M. & Shulman, R. G. (1998) *Proc. Natl. Acad. Sci. USA* **95,** 7715–7720.
7. Rubin, B. D. & Katz, L. C. (1999) *Neuron* **23,** 499–511.
8. Johnson, B. A., Ho, S. L., Xu, Z., Yihan, J. S., Yip, S., Hingco, E. E. & Leon, M. (2002) *J. Comp. Neurol.* **449,** 180–194.
9. Belluscio, L. & Katz, L. C. (2001) *J. Neurosci.* **21,** 2113–2122.
10. Xu, F., Kida, I., Hyder, F. & Shulman, R. G. (2000) *Proc. Natl. Acad. Sci. USA* **97,** 10601–10606.
11. Meister, M. & Bonhoeffer, T. (2001) *J. Neurosci.* **21,** 1351–1360.
12. Uchida, N., Takahashi, Y. K., Tanifuji, M. & Mori, K. (2000) *Nat. Neurosci.* **3,** 1035–1043.
13. Schaefer, M. L., Young, D. A. & Restrepo, D. (2001) *J. Neurosci.* **21,** 2481–2487.
14. Wachowiak, M. & Cohen, L. B. (2001) *Neuron* **32,** 723–735.
15. Fried, H. U., Fuss, S. H. & Korsching, S. I. (2002) *Proc. Natl. Acad. Sci. USA* **99,** 3222–3227.
16. Bozza, T. C. & Kauer, J. S. (1998) *J. Neurosci.* **18,** 4560–4569.
17. Malnic, B., Hirono, J., Sato, T. & Buck, L. B. (1999) *Cell* **96,** 713–723.
18. Zhao, H., Ivic, L., Otaki, J. M., Hashimoto, M., Mikoshiba, K. & Firestein, S. (1998) *Science* **279,** 237–242.
19. Araneda, R. C., Kini, A. D. & Firestein, S. (2000) *Nat. Neurosci.* **3,** 1248–1255.
20. Ma, M. & Shepherd, G. M. (2000) *Proc. Natl. Acad. Sci. USA* **97,** 12869–12874.
21. Johnson, B. A., Woo, C. C., Hingco, E. E., Pham, K. L. & Leon, M. (1999) *J. Comp. Neurol.* **409,** 529–548.
22. Kida, I., Xu, F., Shulman, R. G. & Hyder, F. (2002) *Magn. Reson. Med.* **48,** 570–576.
23. Ressler, K. J., Sullivan, S. L. & Buck, L. B. (1993) *Cell* **73,** 597–609.
24. Vassar, R., Chao, S. K., Sitcheran, R., Nunez, J. M., Vosshall, L. B. & Axel, R. (1994) *Cell* **79,** 981–991.
25. Mombaerts, P., Wang, F., Dulac, C., Chao, S. K., Nemes, A., Mendelsohn, M., Edmondson, J. & Axel, R. (1996) *Cell* **87,** 675–686.
26. Stewart, W. B., Kauer, J. S. & Shepherd, G. M. (1979) *J. Comp. Neurol.* **185,** 715–734.
27. Johnson, B. A. & Leon, M. (2000) *J. Comp. Neurol.* **426,** 330–338.
28. Liu, N., Xu, F., Marenco, L., Hyder, F., Shepherd, G. M. & Miller, P. (2003) *Neuroinformatics*, in press.
29. Strotmann, J., Conzelmann, S., Beck, A., Feinstein, P., Breer, H. & Mombaerts, P. (2000) *J. Neurosci.* **20,** 6927–6938.
30. Cole, L. C. (1949) *Ecology* **30,** 411–424.
31. Ramsden, B. M., Hung, C. P. & Roe, A. W. (2001) *Cereb. Cortex* **11,** 648–665.
32. Spors, H. & Grinvald, A. (2002) *Neuron* **34,** 301–315.
33. Krautwurst, D., Yau, K. W. & Reed, R. R. (1998) *Cell* **95,** 917–926.
34. Touhara, K., Sengoku, S., Inaki, K., Tsuboi, A., Hirono, J., Sato, T., Sakano, H. & Haga, T. (1999) *Proc. Natl. Acad. Sci. USA* **96,** 4040–4045.
35. Singer, M. S. (2000) *Chem. Senses* **25,** 155–165.
36. Sallaz, M. & Jourdan, F. (1992) *NeuroReport* **3,** 833–836.
37. Sallaz, M. & Jourdan, F. (1993) *NeuroReport* **4,** 55–58.
38. Johnson, B. A. & Leon, M. (1996) *J. Comp. Neurol.* **376,** 557–566.
39. Land, L. J. & Shepherd, G. M. (1974) *Brain Res.* **70,** 506–510.
40. Schwob, J. E. & Gottlieb, D. I. (1986) *J. Neurosci.* **6,** 3393–3404.
41. Schoenfeld, T. A. & Knott, T. K. (2002) *J. Chem. Neuroanat.* **24,** 269–285.
42. Frederick, C. B., Udinsky, J. R. & Finch, L. (1994) *Toxicol. Lett.* **70,** 49–56.
43. Andersen, M. E. & Sarangapani, R. (2001) *Inhal. Toxicol.* **13,** 397–414.
44. Keyhani, K., Scherer, P. W. & Mozell, M. M. (1997) *J. Theor. Biol.* **186,** 279–301.
45. Kelly, J. T., Prasad, A. K. & Wexler, A. S. (2000) *J. Appl. Physiol.* **89,** 323–337.
46. Youngentob, S. L., Kent, P. F., Sheehe, P. R., Schwob, J. E. & Tzoumaka, E. (1995) *J. Neurophysiol.* **73,** 387–398.
47. Scott, J. W., Davis, L. M., Shannon, D. & Kaplan, C. (1996) *J. Neurophysiol.* **75,** 2036–2049.
48. Scott, J. W. & Brierley, T. (1999) *Chem. Senses* **24,** 679–690.
49. Baker, H. & Farbman, A. I. (1993) *Neuroscience* **52,** 115–134.
50. Cometto-Muniz, J. E., Cain, W. S. & Abraham, M. H. (1998) *Exp. Brain Res.* **118,** 180–188.
51. Laska, M. & Teubner, P. (1999) *Chem. Senses* **24,** 263–270.
52. Lu, X. C. & Slotnick, B. M. (1998) *Neuroscience* **84,** 849–866.
53. Slotnick, B. & Bodyak, N. (2002) *J. Neurosci.* **22,** 4205–4216.
54. Hyder, F., Kida, I., Behar, K. L., Kennan, R. P., Maciejewski, P. K. & Rothman, D. L. (2001) *NMR Biomed.* **14,** 413–431.
55. Shulman, R. G., Hyder, F. & Rothman, D. L. (2002) *Q. Rev. Biophys.* **35,** 287–325.
56. Laughlin, S. B. (2001) *Curr. Opin. Neurobiol.* **11,** 475–480.
57. Shepherd, G. M. & Greer, C. A. (1998) in *Synaptic Organization in the Brain*, ed. Shepherd, G. M. (Oxford Univ. Press, Oxford), pp. 159–203.